Journal of The Electrochemical Society

Effects of Fluorine Doping on Electrochemical Performance of Spinel-Layered $Li_3Mn_3O_{7.5-x}F_x$ as Cathode Materials for Li-Ion Batteries

Effects of Fluorine Doping on Electrochemical Performance of Spinel-Layered $Li_3Mn_3O_{7.5-x}F_x$ as Cathode Materials for Li-Ion Batteries

Jong Chan Im,[1,=] Ngoc Hung Vu,[2,3,=] Ha Tran Huu,[4] David S. H. Lee,[5] and Won Bin Im[4,z]

[1] *School of Materials Science and Engineering, Chonnam National University, Buk-gu, Gwangju 61186, Korea*
[2] *Faculty of Biotechnology, Chemistry and Environmental Engineering, Phenikaa University, Hanoi 10000, Vietnam*
[3] *Phenikaa Research and Technology Institute (PRATI), A&A Green Phoenix Group, Hanoi 10000, Vietnam*
[4] *Division of Materials Science and Engineering, Hanyang University, Seongdong-gu, Seoul 04763, Korea*
[5] *Department of Chemical Engineering, Missouri University of Science and Technology, Rolla, Missouri 65409, USA*

A simple synthesis procedure for solid-state reactions at an intermediate temperature (500°C) is applied to synthesize F-doped spinel-layered $0.5Li_2MnO_3$•$0.5Li_4Mn_5O_{12}$ ($Li_3Mn_3O_{7.5-x}F_x$ with $x = 0$, 0.05, 0.1, and 0.2). The F-doping does not affect the crystal structure or the morphology of the pristine sample. However, F-doping increases the Mn^{3+} content, leading to an improved electronic conductivity and a lower charge-transfer resistance. In addition, F-doping also reduces the difference of voltage between the oxidation and reduction processes, and enhances the Li^+ diffusion coefficient (with a maximum four times higher than that of the pristine sample). Consequently, the capacity and rate capability of the cathode are improved by F-doping (the $x = 0.1$ sample can provide a high capacity of 300 mAh g^{-1} at C/10).

 [DOI: 10.1149/2.0861908jes]

Manuscript submitted March 5, 2019; revised manuscript received April 26, 2019. Published May 8, 2019.

High capacity and secure cathode materials for Li-ion batteries (LIBs) are greatly important for the development of next generation electric vehicles and energy storage systems. Although $LiMn_2O_4$ and $LiFePO_4$ have the advantages of being abundant and environmentally friendly, they have low practical capacities, 148 and 170 mAh g^{-1}, respectively.[1] Therefore, substantial efforts have been made to discover alternative cathode materials to increase the energy density of the batteries system.[2,3] Moreover, cathode materials based on Li–Mn–O systems have attracted much attention due to their low cost, ease of synthesis, great stability, and environmental friendliness.[4] The single phase of Mn-based compounds, such as Li_2MnO_3 and $Li_4Mn_5O_{12}$, cannot be used as a cathode material for LIBs due to the following reasons. First, $Li_4Mn_5O_{12}$ has a flat 3V plateau and relatively high theoretical capacity (163 mAh g^{-1}), but the Li^+ cannot be extracted from the first charge as all of the Mn is in the +4 oxidation state. Second, $Li_4Mn_5O_{12}$ is decomposed into $LiMn_2O_4$ and Li_2MnO_3 at high temperatures, (>700°C) and therefore, it is difficult to synthesize a single phase.[5] On the other hand, Li_2MnO_3 cathode material is hazardous and has a low conductivity and fast voltage decay.[6] These disadvantages can be overcome by designing a composite structure of xLi_2MnO_3·(1-x)$Li_4Mn_5O_{12}$. Fig. 1 shows the structure of Li_2MnO_3 and $Li_4Mn_5O_{12}$ ($Li_{1.33}Mn_{1.67}O_4$). In the Li_2MnO_3 structure, both Li and Mn occupy octahedral site while in the $Li_4Mn_5O_{12}$ structure, Mn occupy octahedral sites and most of Li occupy tetrahedral sites of oxygen close-packed structure.[7,8] In addition, in the ideal Li_2MnO_3, Li and Mn are ordered inside the layers, while they are randomly distributed in the 16*d* sites of the $Li_4Mn_5O_{12}$ spinel.[8] Due to the similarity of the oxygen sub-lattices and the ease of transformation between the two structures depending synthesis conditions, the composite structures can be formed at atomic level. The introduction of spinel phase into the compound enhances the first Coulombic efficiency (CE), rate capability, and cycle performance of the composite cathode.[3,7,9–14] Thackeray et al.[15] reported layered-spinel systems of xLi_2MnO_3 ·(1-x)$Li_{1+y}Mn_{2-y}O_4$ ($0 < x < 1$; $0 \leq y \leq 0.33$), which can provide very high capacities ~270 mAh g^{-1}. Cao et al.[16] also reported $0.5Li_2MnO_3$·$0.5Li_4Mn_5O_{12}$ ($Li_3Mn_3O_{7.5}$) nanotubes synthesized by a self-templating method. However, the capacity of this cathode was less than 200 mAh g^{-1} at C/5 with poor cycling stability.

To stabilize the structure and enhance the electrochemical properties, F-doping/substitution for O is a widely used strategy.[17–19] Luo et al.[20] reported that F-doping reduces the oxidation state of Mn, leading to an increased capacity of spinel $LiMn_{2-2y}Li_yM_yO_{4-x}F_x$ (M = Fe, Co, Zn). Dong et al.[21] reported that F-substitution for O weakens the Li–O bond, induces more Mn^{3+} and O vacancies. This would reduce the energy barrier of Li^+ from the crystal structure and improve the electronic transmission performance. In addition, F-doping can protect the electrode from HF attack.[22] In this work, we prepared F-doped $0.5Li_2MnO_3$·$0.5Li_4Mn_5O_{12}$ [$Li_3Mn_3O_{7.5-x}F_x$ ($x = 0$, 0.05, 0.1, and 0.2)] materials.

To study the effects of F-doping on the structure, morphologies, and electrochemical properties of the cathode materials, X-ray diffraction (XRD), field emission scanning electron microscopy (FE-SEM), X-ray photoelectron spectroscopy (XPS), galvanostatic charge-discharge measurement, cyclic voltammetry (CV), electrochemical impedance spectroscopy (EIS) were performed.

Experimental

Preparation of the materials.—The $Li_3Mn_3O_{7.5-x}F_x$ were synthesized by a solid-state reaction. Appropriate ratios of dried $LiOH{\cdot}H_2O$, Mn_2CO_3 and NH_4F powders were mixed for 20 min using an agate mortar. The obtained mixtures were then fired at 500°C for 12 h in air. The F contents in the composite $Li_3Mn_3O_{7.5-x}F_x$ were varied ($x = 0$, 0.05, 0.1, and 0.2) by controlling the amount of NH_4F.

Structural and physical characterization.—The XRD were measured by Shimadzu X-ray diffractometer with Ni-filtered Cu Kα radiation (λ = 1.5406 Å) at 40 kV and 30mA with a step of 0.02° within the scanning angle of 2θ (from 10 to 80°). The FESEM (S-4700, Hitachi) were used to check morphologies of the products. The chemical states of the elements were characterized by XPS (VG MultiLab 2000, Thermo Scientific).

Electrochemical measurements.—To study the electrochemical properties of synthesized samples, coin cells were fabricated. The cathodes, which contained the active material, Ketjen black (a conductive carbon), and a TAB (teflonized acetylene black as a binder), in the mass ratio 70:10:20, were mixed, pressed onto stainless steel mesh, and then dried under vacuum at 120°C for 12 h. The electrolyte was 1 M $LiPF_6$ in a 1:1 mixture of ethylene carbonate (EC)/dimethyl

[=]These authors contributed equally to this work.
[z]E-mail: imwonbin@hanyang.ac.kr

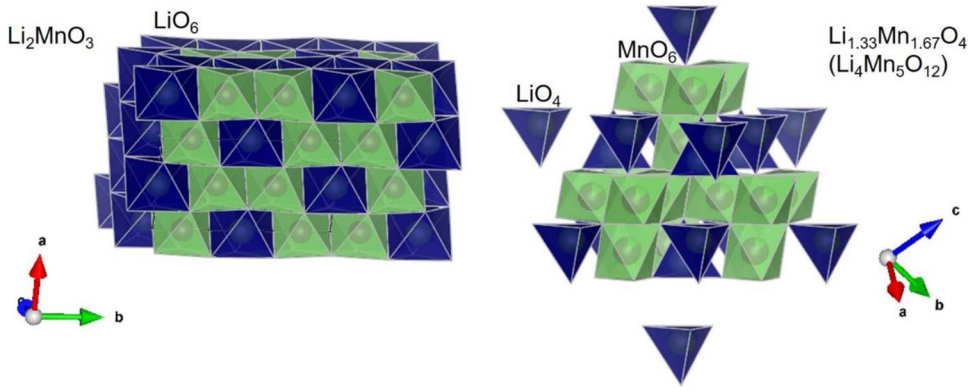

Figure 1. Schematic of a Li_2MnO_3 layered structure and a $Li_4Mn_5O_{12}$ spinel structure. The octahedron of Mn and octahedron (tetrahedron) of Li are shown in green and dark blue color, respectively.

carbonate (DMC). The coin cells were assembled in a glove box filled with pure argon gas. A NAGANO BTS-2004H battery charger was used to check the charge-discharge performance of the cathodes between 2.0 and 4.8 V. The CV and EIS measurements were obtained with an Autolab. A scan rate of 0.1 mV s^{-1} between 2.0 and 4.8 V vs. Li^+/Li for CV and a voltage of 5 mV amplitude over the frequency range 100 kHz to 0.01 Hz for EIS were set up.

Results and Discussion

The XRD patterns of the synthesized samples are shown in Fig. 2. The diffraction peaks of all samples indicate the presence of two phases, which are $Li_4Mn_5O_{12}$ (cubic spinel, *Fd3m* space group) and Li_2MnO_3 (monoclinic, *C*/2*m* space group). The layered peaks are overlapped by the spinel peaks because they have similar cubic close-packed oxygen sites.[3,23] However, the unique superlattice peak at 20.5° of $(020)_L$ plane (where *L* stands for layered) confirms the presence of a layered phase. Moreover, the peak at 65.5° which is assigned to the $(060)_L$ plane of the Li_2MnO_3 phase, also appears in all of the samples. Due to the firing temperature is low, the particles might have small sizes and low crystallinity. Therefore, the diffraction peaks of all samples are broad. The F-doped samples exhibit similar peaks as the pristine sample, indicating there is no change to the crystal structure after F-doping. It is noteworthy that the F-doping of Li_2MnO_3 slightly expanded the Li^+ transmission channel and induced $Li_4Mn_5O_{12}$ formation.[21]

Figs. 3a, 3b, 3c shows the SEM images of all samples for the evaluation of their morphologies and particle sizes. The primary particles in sizes ~50–80 nm are agglomerated to form larger secondary particles in all of the samples. According to Li et al.,[24] F-doping accelerates the growth of particles with a two-step firing. In this study, at a low synthesis temperature and one step firing, the morphologies of the particles did not change significantly. Figs. 3e, 3f, 3g, 3h, 3i exhibits the

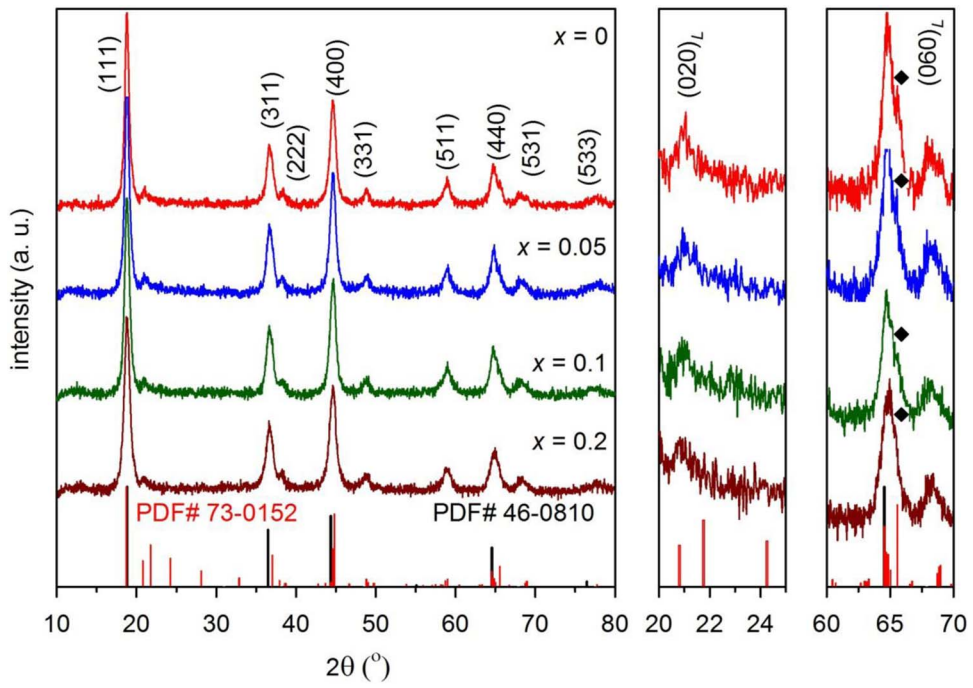

Figure 2. XRD patterns of the $x = 0$, 0.05, 0.1, and 0.2 samples indexed with standard Li_2MnO_3 of PDF No. 73-0152, space group *C*/2*m*; and $Li_4Mn_5O_{12}$ of PDF No. 46-0810, space group *Fd3m*. The XRD pattern with enlarged Bragg angle ranges of 20–25° and 60–70° are shown to highlight the presence of the layered peaks denoted by the $(020)_L$ and $(060)_L$ planes.

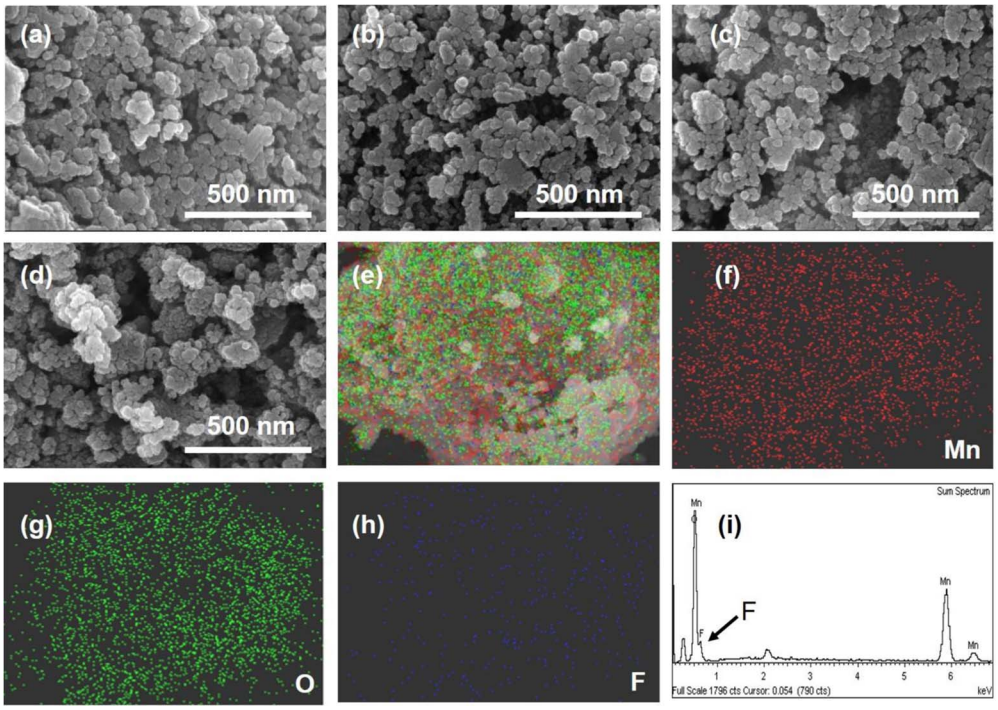

Figure 3. FESEM images of the $x = $ (a) 0, (b) 0.05, (c) 0.1, and (d) 0.2 samples. (e) Element mapping image of three elements and for (f) Mn, (g) O, and (h) F of the $x = 0.1$ sample. (i) EDX profiles of the $x = 0.1$ sample.

EDS mappings of a secondary particle of the $x = 0.1$ sample. F were detected on the particle, in addition to the other major components of the material (Mn, O), and were uniformly distributed. This indicates that F was successfully incorporated into the compound.

To further confirm the presence of F-doping and determine the oxidation state of each element in the compounds, an XPS analysis was performed and is shown in Fig. 4. The Mn 2*p* core-level spectrum as shown in Fig. 4a included two signals because of spin-orbital splitting. They were allocated to Mn $2p_{3/2}$ and Mn $2p_{1/2}$[25] and all samples did not have their values less than 11.5 eV. For the pristine sample, the binding energy of Mn $2p_{3/2}$ was 642.45 eV, which is very similar to Mn $2p_{3/2}$ of single phase Li_2MnO_3[21] and $Li_4Mn_5O_{12}$,[26] suggesting most of the Mn is in the +4 oxidation state, with a small quantity of Mn^{3+}. For the F-doped samples, and increasing *x*, these peaks shift to lower binding energies and the value of the spin orbit splitting decreases, indicating the generation of more Mn^{3+} ions. The Mn^{3+} ions would provide an improved electrochemical properties of the samples by increasing the electronic conductivity and acting as the activated center (which can be seen in EIS data).[21] Fig. 4b shows the F 1*s* core-level spectrum of the samples. As the amount of incorporated F increases, the intensity of the F 1*s* peaks gradually increase. The measured binding energy for F 1*s* was ~684.5 eV, indicating that F exists in the compound as F^{-}[24].

The charge-discharge curve of all samples for the 1st, 3rd, 50th are shown in Fig. 5. As can be seen from that, during the first charge, four samples exhibited a similar behavior, with a slope from 3.8 to 4.4 V, a plateau at ~4.5 V, and a slope from 4.6 to 4.8 V. The sloped region from 3.8 to 4.4 V was caused by the oxidation of a small amount of Mn^{3+} in the $Li_4Mn_5O_{12}$ component. The plateau at ~4.5 V is associated with the electrochemical activation of the Li_2MnO_3 component.[3] This plateau is longer in the F-doped samples than in the pristine sample, indicating the F-doped samples have more efficient activation than the pristine sample has. Therefore, it can provide a very high discharge capacities of 288 mA h g^{-1} ($x = 0.1$ sample) while the pristine sample can deliver only 238 mA hg^{-1}. The sloped region from 4.6 to 4.8 V relates to the oxidation of electrolyte and formed cathode electrolyte interphase layer.

Upon discharge, there is one quasi-plateau from 4.4 to 3.8 V, one plateau at 2.8 V, and two sloping regions (3.8 to 2.8 V and 2.8 to 2 V). The quasi-plateau is the contribution of layered and spinel phase accompanying the reduction of Mn^{4+} to Mn^{3+}. The sloping region from 3.8 to 2.8 V is typical for the Li_2MnO_3 phase, while the plateau at 2.8 V is a feature of the $Li_4Mn_5O_{12}$ phase (the insertion of Li into 16*c* empty sites of the spinel structure). The last sloping region contains contributions of both phases. The F-doped samples exhibited a higher capacity than the pristine sample because: 1) the increased amount of Mn^{3+} in the F-doped samples, which not only facilitates migration of polarons but also supports a more activated center, led to an increase in the electronic conductivity,[21] and 2) F-doping facilitates the activation of the Li_2MnO_3 component, so that more Li^{+} can be extracted. For the 3rd cycle, the capacity increased due to the activation of the Li_2MnO_3 phase and the $x = 0.1$ sample exhibited the highest discharge capacity, ~300 mAh g^{-1}. For the 50th cycle, the capacity decreased and would be discussed later.

The performance of the materials for different C-rates was shown in Fig. 6a. At low C-rate of C/10 (current density of 1 C = 230 mA g^{-1}), all samples exhibited slightly different discharge capacities. However, at high C-rates, the discharge capacities of the F-doped samples were significantly higher than those of the pristine sample. The improvement in rate capabilities of the F-doped samples will be elucidated in EIS data. In particular, the $x = 0.1$ sample delivered the highest capacities of 280, 270, 240, 210, 190, and 163 mAh g^{-1} at C/10, C/5, C/2, 1C, 2C, and 5C, respectively. Compared with the pristine sample at 5C, the $x = 0.1$ sample delivered a higher capacity of 116%. In overall, the F-doped samples facilitated high capacities at rates 2.5 times higher than those of the pristine sample.

Fig. 6b shows the cycling performances of the cathodes in a voltage range of 2.0–4.8 V at C/2. All samples were activated at C/10 for three cycles. The capacities of the $x = 0.05$ and 0.1 samples were ~243 mAh g^{-1}, while the $x = 0.2$ sample provided a capacity of 231 mAh g^{-1}. For the pristine sample, maximal capacities of 215 mAh g^{-1} were attained. The capacity of the $x = 0.1$ sample was superior (13% higher) than that of the pristine sample. All of the F-doped samples had similar capacities. The higher capacity of the F-doped samples

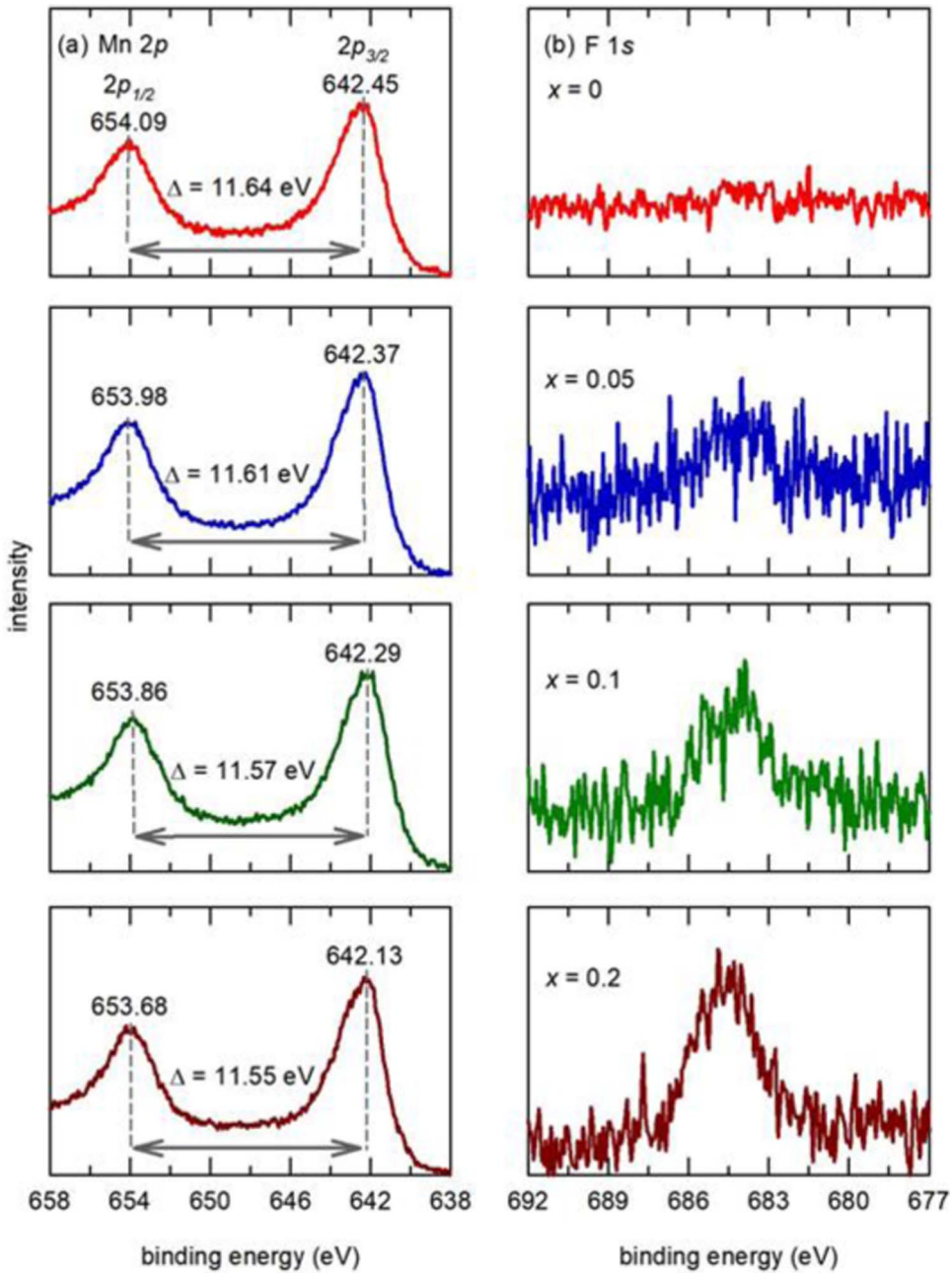

Figure 4. XPS spectra of (a) Mn 2*p* and (b) F 1*s* of the $x = 0$, 0.05, 0.1, and 0.2 samples.

is explained by the improved conductivity due to the existence of more Mn^{3+}. The capacity retention for $x = 0$, 0.05, 0.1, and 0.2 were 69.35, 70.78, 70.8, and 73.08%, respectively. The poor cycling stability of these composites was caused by the inherent properties of Li_2MnO_3 that transforms to the spinel phase during cycling, which agrees with other reports.[15,16] However, F-doping can improve the cycling stability for electrode materials because it stabilizes the electrode/electrolyte interface. The CE for the first cycle of all samples surpassed 100% due to the presence of the spinel phase. This phase has empty octahedral 16*c* sites so excess Li can be accommodated during discharge into these sites of the spinel lattice accompanied by the reduction of Mn.[3] The CE of all samples were close to 100% in the subsequent cycles, exhibiting insignificant energy loss during charge and discharge.

The CV results of the samples were measured in the voltage range from 2.0 to 4.8 V and a scan rate of 0.1 mV s^{-1}; the cyclic voltammograms are shown in Fig. 7. In the first charge of the samples, the peak at ~4.0 V and the peak at ~4.5 V are attributed to the oxidation of Mn^{3+} and the oxygen evolution and Li^+ extraction from Li_2MnO_3 component, respectively.[25] For the first discharge, the peaks at ~4 V of all of the samples correspond to the reduction of Mn^{4+} in the layered and spinel phases, while the peaks at 2.8 V corresponds to the reduction of Mn^{4+} in the spinel phase. The peaks of the F-doped samples shifted to higher potentials and were stronger, compared to those of the pristine sample, caused by the positive effects of F (increasing conductivity) (2.75 and 2.71 V for the $x = 0.1$ and 0 samples, respectively). For the next two cycles, two types of oxidation/reduction couples at ~3/2.8 V and 4.1/4 V in all of the samples are shifted to higher potentials. These peaks match the charge-discharge curves (Fig. 4). The difference of voltage between the oxidation and reduction peaks is smaller for the $x = 0.1$ sample ($\Delta = 0.233$ V) than that of the pristine sample ($\Delta = 0.243$ V), indicating a better Li^+ diffusion due to the F-doping effect.

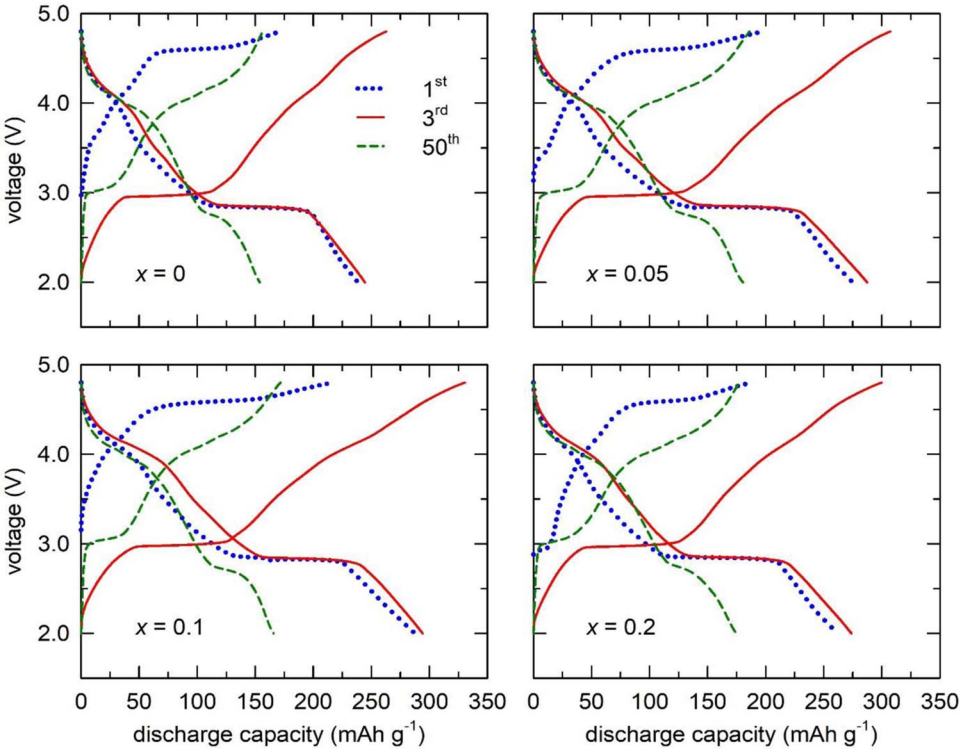

Figure 5. Voltage profiles for the 1st, 3rd, and 50th cycle of the $x =$ (a) 0, (b) 0.05, (c) 0.1, and (d) 0.2 samples.

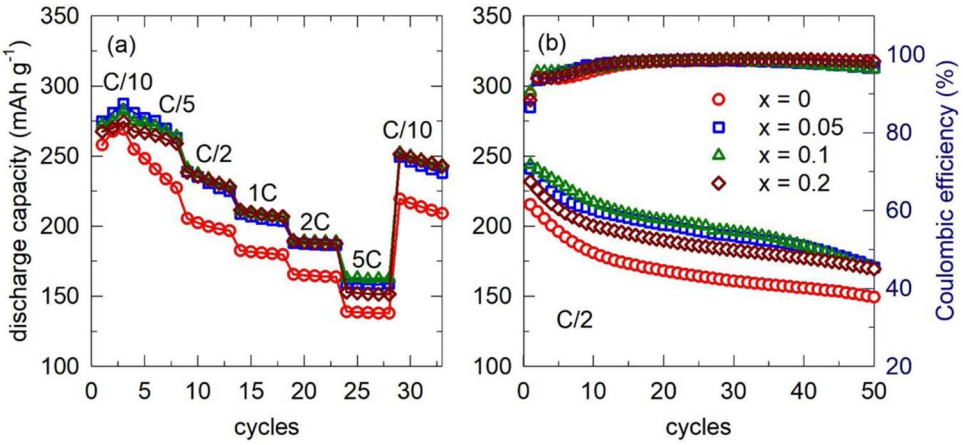

Figure 6. (a) Cycling stability curves at different C-rates and at (b) C/2 of the $x = 0$, 0.05, 0.1, and 0.2 samples.

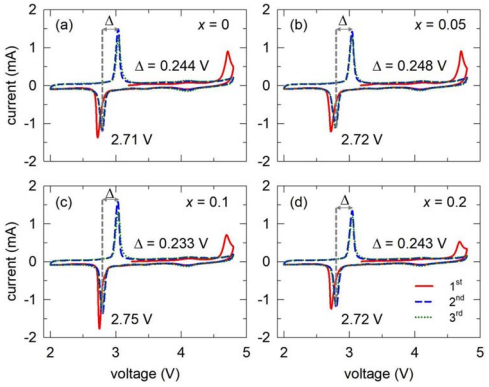

Figure 7. Cyclic voltammograms of the $x =$ (a) 0, (b) 0.05, (c) 0.1, and (d) 0.2 samples.

By using EIS, the electrochemical performance of these cathodes was further investigated (Fig. 8). The Nyquist plots of the original cathodes showed two features. The first one is a semicircle which is attributed to the charge-transfer resistance (R_{ct}) in the medium-frequency region. The second one is a sloped line in the low-frequency region, which is associated with the Li^+ diffusion through the cathodes (Warburg diffusion).[25] The R_{ct} of the $x = 0.1$ sample (55 Ω) is the lowest. The R_{ct} of the $x = 0.05$ and 0.2 samples were 78 Ω, and lower than that of the pristine sample (90 Ω). A lower value of R_{ct} causes an increase in the capacity in the F-doped samples. Moreover, the Li^+ diffusion coefficients of all of the samples are provided in Table I and were calculated by:

$$D = R^2T^2/2An^4F^4C^2\sigma^2 \quad [1]$$

where R, T, and A are the gas constant, the absolute temperature, and the surface area of the cathode, respectively. The parameters n, F, and C are the number of electrons transferred in the half-reaction for the

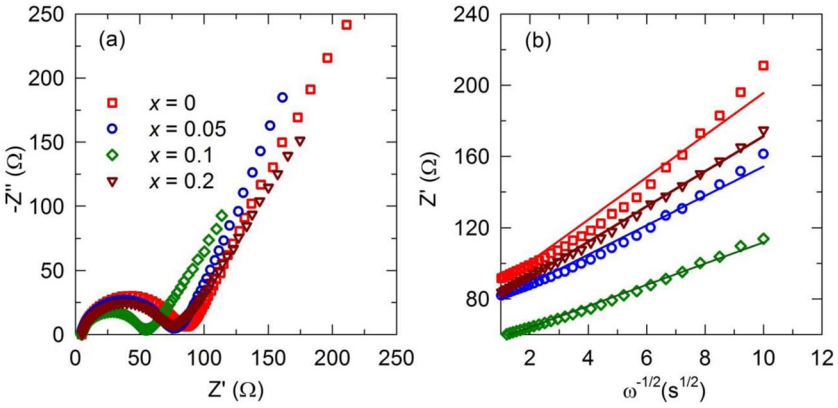

Figure 8. (a) EIS and (b) real parts of the complex impedance versus $\omega^{-1/2}$ of $x = 0$, 0.05, 0.1, and 0.2 samples before cycling.

Table I. Warburg factor and diffusion coefficient of $Li_3Mn_3O_{7.5-x}F_x$ ($x = 0$, 0.05, 0.1, and 0.2).

sample	σ	D_{Li+} ($cm^2\ s^{-1}$)
$x = 0$	11.838	4.40×10^{-11}
$x = 0.05$	8.22	9.13×10^{-11}
$x = 0.1$	5.96	1.74×10^{-10}
$x = 0.2$	9.853	6.36×10^{-11}

redox couple, the Faraday constant, and the concentration of Li ions in the solid, respectively. D is the diffusion coefficient ($cm^2\ s^{-1}$), and σ is the Warburg factor, which is relative to Z'. σ can be obtained from the slope of the lines in Fig. 8b:

$$Z' = R_D + R_L + \sigma\omega^{-1/2}. \quad [2]$$

From the results in Table I, the $x = 0.1$ sample has the highest Li^+ diffusion coefficient (1.74×10^{-10} $cm^2\ s^{-1}$). The $x = 0.05$ and 0.1 samples also have Li^+ diffusion coefficients greater than that of the pristine sample. This phenomenon can be explained by the weakening Li–O bond in F-doped samples that would favor the Li^+ diffusion, resulting an increased Li^+ diffusion coefficient. However, for the case $x = 0.2$, with a large amount of F-doping, the Li^+ diffusion was prevented. The total performance rates were in the sequence $x = 0.1 > x = 0.05 > x = 0.2 > x = 0$ for all of the investigated C-rates because of the effects of F-doping.

Conclusions

Low cost and high capacity $Li_3Mn_3O_{7.5-x}F_x$ cathode materials can be obtained by F-doping. XRD and SEM data showed that F is included into the structure, and F-doping does not change the morphology of the pristine sample. The XPS analysis revealed that F-doping increased the Mn^{3+} content. Finally, the electrochemical analyses indicated that F-doping enhanced the capacity (up to 13% higher than that of the pristine sample) and rate capability (at rates 2.5 times higher than that of the pristine sample) by facilitating the activation of Li_2MnO_3, lowering the charge-transfer resistance, and improving the Li^+ diffusion coefficient. More importantly, the F-doping exhibited positive effects in terms of capacity retention, and can be applied to similar spinel-layered systems.

Acknowledgments

This research was supported by the Basic Science Research Program through the National Research Foundation of Korea (NRF) funded by the Ministry of Science, ICT, and Future Planning (2017R1A2B3011967). This research was also supported by the NRF grant funded by the Korean Government (MSIT), (NRF-2018R1A5A1025224).

ORCID

Ngoc Hung Vu https://orcid.org/0000-0001-7203-5745
Won Bin Im https://orcid.org/0000-0003-2473-4714

References

1. C. Julien, A. Mauger, K. Zaghib, and H. Groult, *Inorganics*, **2**, 132 (2014).
2. N. H. Vu, P. Arunkumar, S. Won, H. J. Kim, S. Unithrattil, Y. Oh, J.-W. Lee, and W. B. Im, *Electrochimica Acta*, **225**, 458 (2017).
3. N. H. Vu, P. Arunkumar, J. C. Im, D. T. Ngo, H. T. T. Le, C.-J. Park, and W. B. Im, *Journal of Materials Chemistry A*, (2017).
4. M. M. Thackeray, C. S. Johnson, J. T. Vaughey, N. Li, and S. A. Hackney, *Journal of Materials Chemistry*, **15**, 2257 (2005).
5. T. Takada, H. Hayakawa, E. Akiba, F. Izumi, and B. C. Chakoumakos, *Journal of Power Sources*, **68**, 613 (1997).
6. Y. Denis, K. Yanagida, Y. Kato, and H. Nakamura, *Journal of The Electrochemical Society*, **156**, A417 (2009).
7. B. R. Long, J. R. Croy, J. S. Park, J. Wen, D. J. Miller, and M. M. Thackeray, *Journal of The Electrochemical Society*, **161**, A2160 (2014).
8. S. Ivanova, E. Zhecheva, D. Nihtianova, and R. Stoyanova, *Journal of Materials Science*, **46**, 7098 (2011).
9. D. Kim, G. Sandi, J. R. Croy, K. G. Gallagher, S.-H. Kang, E. Lee, M. D. Slater, C. S. Johnson, and M. M. Thackeray, *Journal of The Electrochemical Society*, **160**, A31 (2013).
10. A. Bhaskar, S. Krueger, V. Siozios, J. Li, S. Nowak, and M. Winter, *Advanced Energy Materials*, **5**, 1401156 (2015).
11. N. H. Vu, P. Arunkumar, J. C. Im, and W. B. Im, *Journal of Alloys and Compounds*, **704**, 459 (2017).
12. N. H. Vu, P. Arunkumar, and W. B. Im, *Scientific Reports*, **7**, 45579 (2017).
13. F. Wu, N. Li, Y. Su, H. Shou, L. Bao, W. Yang, L. Zhang, R. An, and S. Chen, *Advanced Materials*, **25**, 3722 (2013).
14. P. K. Nayak, J. Grinblat, M. D. Levi, O. Haik, E. Levi, M. Talianker, B. Markovsky, Y.-K. Sun, and D. Aurbach, *Chemistry of Materials*, **27**, 2600 (2015).
15. C. S. Johnson, N. Li, J. T. Vaughey, S. A. Hackney, and M. M. Thackeray, *Electrochemistry Communications*, **7**, 528 (2005).
16. J. Cao, J. Xie, G. Cao, T. Zhu, X. Zhao, and S. Zhang, *Electrochimica Acta*, **111**, 447 (2013).
17. X. Hu, H. Guo, J. Wang, Z. Wang, X. Li, Q. Hu, and W. Peng, *Ceramics International*, **44**, 14370 (2018).
18. B. Jiang, B. Luo, J. Li, P. Peng, J. Chen, L. Chu, Y. Li, and M. Li, *Ceramics International*, **45**, 160 (2019).
19. D. Jugović, M. Mitrić, M. Milović, N. Cvjetićanin, B. Jokić, A. Umićević, and D. Uskoković, *Ceramics International*, **43**, 3224 (2017).
20. Q. Luo and A. Manthiram, *Journal of The Electrochemical Society*, **156**, A84 (2009).
21. X. Dong, Y. Xu, S. Yan, S. Mao, L. Xiong, and X. Sun, *Journal of Materials Chemistry A*, **3**, 670 (2015).
22. C. Gao, J. Zhou, G. Liu, and L. Wang, *Journal of Alloys and Compounds*, **727**, 501 (2017).
23. N. H. Vu, S. Unithrattil, V. H. Hoang, S. Chun, and W. B. Im, *Journal of Power Sources*, **355**, 134 (2017).
24. X. Li, Z. Xie, W. Liu, W. Ge, H. Wang, and M. Qu, *Electrochimica Acta*, **174**, 1122 (2015).
25. N. H. Vu, J. C. Im, S. Unithrattil, and W. B. Im, *Journal of Materials Chemistry A*, (2018).
26. Y. Tian, D. Chen, X. Jiao, and Y. Duan, *Chemical Communications*, 2072 (2007).